China Ocean Engineering, Vol.18, No.4, pp.551 - 566

Numerical Investigation on the Generation and Propagation of Irregular Waves in A Two-Dimensional Wave Tank*

Ruey-syan SHIH[a, 1], Chung-ren CHOU[b] and John Z. YIM[b]

[a]*Department of Civil Engineering, Tung Nan Institute of Technology, 22202 Village Shen Keng, Taipei, R.O.C*

[b]*Department of Harbour and River Engineering, Taiwan Ocean University, 20224 Keelung, R.O.C*

(Received 9 June 2004; accepted 30 August 2004)

ABSTRACT

The modeling of generation and subsequent propagation of irregular waves in a numerical wave flume is performed by mean of the boundary element method. Random waves are generated by a piston-type wave generator at one end of the flume with the Mitsuyasu-Bretschneider spectrum used as the target spectrum for the generation. An artificial absorbing beach is placed at the other end of the flume to minimize wave reflection. Surface fluctuations are described by use of the Lagrangian description, and finite difference is adopted for the approximation of time derivative. To monitor the developments of the waves, a number of pseudo wave gauges are installed along the tank. Through comparison of the spectra from those gauges with the target spectrum, satisfactory results can be obtained from the present numerical scheme.

Key words: *numerical wave tank*; *irregular waves*; *absorbing beach*

1. Introduction

Coastal and Oceanic structures are constructed to endure the most severe environmental forces during their lifetime. Of all possible forces, wave forces are often considered to be the dominant ones.

Wave forces acting on a structure can be determined either by measurement through physical model tests or by use of numerical algorithms. In the latter case it is customary to estimate wave forces with the Morison equation. The major problem associated with the Morrison equation is that, however, the drag force is in quadrature with the horizontal water particle velocity on the free surface, which is not known from existing wave theories. Various schemes have been proposed to extrapolate water particle velocities from the still water level to the free surface. A fairly detailed comparison of the merits and demerits of these methods can be found in Gudmestad and Spidsøe (1990; see also Tørum and Skjelbreia, 1990). On the other hand, forces due to breaking waves are believed to cause more damage than unbroken ones. However, owing to the turbulent nature, it is even more difficult, if not impossible, to measure broken wave forces acting on a structure.

Most of the above-mentioned difficulties can be overcome when a researcher knows the properties of the waves along their track of evolution all the time. There is a possibility that such opportunities can be provided by a numerical wave tank. In the tank, waves are initially generated by a pseudo

* The work was financially supported by the financial aid of the Science Council, Taiwan, Project Nos. NSC - 89 - 2611 - E - 019 - 027 (CRC) and NSC - 89 - 2611 - E - 019 - 058 (JZY).

1 Corresponding author. E-mail: rsshih@mail.tnit.edu.tw

wavemaker; the subsequent developments of these waves along the tank are modelled by solving some governing equations.

Although started some thirty years ago, numerical estimation of wave characteristics through numerical models has been largely developed only quite recently due to the rapid advance in computer technology in the last decade. The generation of nonlinear waves with boundary integral equations was subsequently considered by Brorsen and Larsen (1987). Sugino and Tosaka (1990) used the boundary element method to analyze the generation, propagation, and subsequent deformation of solitary waves in a water tank. Invoking Green's theorem, Isaacson *et al.* (1993) used a time-domain second-order method to simulate the propagation of nonlinear waves in a flume. Chou and Shih (1996a, 1996b) developed a wave model using the boundary element method for modeling the generation and deformation of both periodical and solitary waves; their scheme was based on the Lagrangian description of fluid with time derivative approximated by finite differencing.

The majority of the above-mentioned researches deal with the generation and propagation of regular waves. Very often, waves are of the monochromatic nature, i.e., they have one "carrier frequency". However, like many natural phenomena in the world, water waves are nonlinear. Subjected to the nonlinear boundary conditions, high harmonics will be generated and regular waves tend to deform in the course of development. To model this effect, Grilli and Horrillo (1997) used fully nonlinear boundary conditions. In a recent paper, Williams (1999) considered the generation and propagation of second-order Stokes waves. A novel second-order radiation boundary condition was applied at the far-field boundary. The results were found to be satisfactory when compared with experiments.

However, waves in the ocean are generally both random and quasi- regular, and the wave profile varies constantly with time and in a random fashion. Consequently, the properties of surface waves are not readily defined on a wave-by-wave basis. On the other hand, a realistic numerical wave tank should be capable of modeling the generation and development of irregular waves.

Recently, Xu and Baddour (1999) reviewed the results of simulating the propagation of nonlinear, irregular waves in two- and three-dimensional numerical basins. The basins were quipped with wave -absorbing beaches. In their model, the so-called Green-Naghdi fluid sheets theory was used. Chou *et al.* (2001) modelled the generation and propagation of irregular waves in a 2D wave basin, and a spectrum of the Mitsuyasu-Bretschneider type is chosen as the target one. However, probably owing to the numerical dissipation of the scheme, only waves with large wavelengths were found to reach the beach.

The scheme of Chou *et al.* (2001) is further improved in this paper. Its application to the generation of irregular waves reveals that the improved numerical scheme is capable of describing the propagation of irregular waves satisfactorily.

2. Numerical Scheme

2.1 Governing Equations and Basic Assumptions

As shown schematically in Fig. 1, the numerical wave flume is confined in a region composed of

a piston type wave generator located at the right, the undisturbed free water surface, an impermeable vertical wall and an impermeable bottom. Cartesian coordinates are employed; the origin is located on the still water surface with the z-axis pointing positively upwards. Unlike Williams (1999), who used a semi-infinite boundary condition, we have adopted a vertical wall at the left end of the flume as boundary in our analysis so as to bear more resemblance to the physical wave generation. The regime of interest is bounded by the pseudo wave board Γ_1, the free water surface Γ_2, the vertical wall Γ_3, and the impermeable bottom floor Γ_4. The boundaries are discretized as linear elements.

The fluid within the region is conventionally assumed to be incompressible, inviscid, and irrotational. According to Green's second identity, the velocity potential $\Phi(x, z, t)$ must satisfy the following Laplace equation:

$$\frac{\partial^2 \Phi}{\partial x^2} + \frac{\partial^2 \Phi}{\partial z^2} = 0. \tag{1}$$

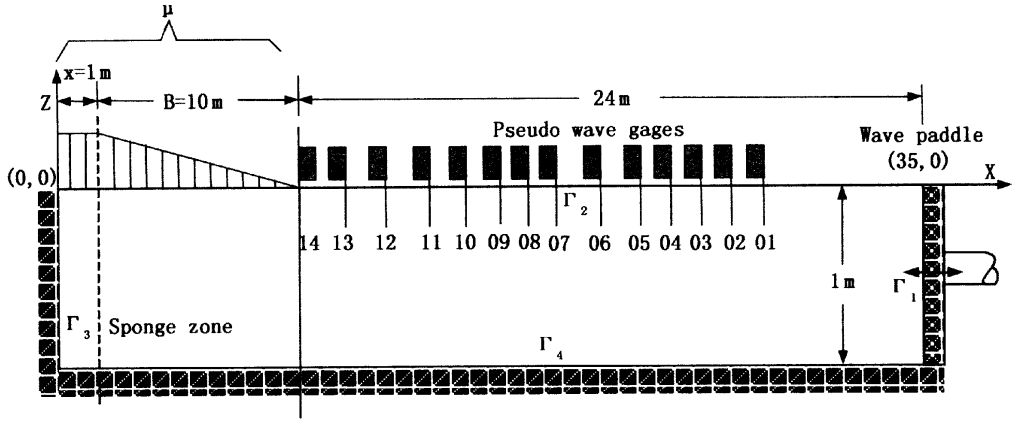

Fig. 1. Definition sketch of the numerical wave flume.

2.2 Boundary Conditions

The horizontal and vertical components of the water particle velocity, u and, w can be expressed as:

$$u = \frac{Dx}{Dt} = \frac{\partial \Phi}{\partial x}, \tag{2}$$

and

$$w = \frac{Dz}{Dt} = \frac{\partial \Phi}{\partial z}. \tag{3}$$

In the Lagrangian form, the dynamic free-surface boundary conditions is then written as:

$$\frac{D\Phi}{Dt} + g\zeta - \frac{1}{2}\left[\left(\frac{\partial \Phi}{\partial x}\right)^2 + \left(\frac{\partial \Phi}{\partial z}\right)^2\right] + \frac{P}{\rho} = 0 \tag{4}$$

where, D( ) is the Lagrangian derivative; g is the gravitational acceleration; with ζ representing the surface fluctuation; ρ is the density of water; and P is the pressure on the water surface.

The boundary condition on the wave-paddle is obtained by matching the horizontal velocities of the paddle and those of the fluid through the following association:

$$\bar{\Phi} = \frac{\partial \Phi}{\partial n} = - U(t), \quad \text{on} \quad \Gamma_1 \tag{5}$$

where n is the unit outward normal vector.

Since the particle velocity is null in the normal direction on the impermeable vertical wall and the bottom floor, the condition is prescribed as:

$$\frac{\partial \Phi}{\partial n} = 0, \qquad \text{on } \Gamma_3 \text{ and } \Gamma_4. \tag{6}$$

2.3 Random Wave Simulation

The Bretschneider-Mitsuyasu spectrum is used as the target spectrum for the generation of irregular waves, which can be expressed as:

$$S_0(f) = 0.257 H_{1/3}^2 T_{1/3}^{-4} f^{-5} \exp[-1.03(T_{1/3} f)^{-4}] \tag{7}$$

where $H_{1/3}$ is the significant wave height; $T_{1/3}$ is the significant wave period; and f is the frequency.

According to Goda (2000), the spectral peak frequency, f_p, is related to the significant wave period, T_p:

$$f_p = 1/T_p \tag{8}$$

where $T_p \cong 1.05 T_{1/3}$. Similar to the case of physical applications of the wave generation theory, a transfer function must be multiplied to yield the spectrum for the motion of the numerical wave generator, thus,

$$S(f) = \alpha(f)^2 \cdot S_0(f) \tag{9}$$

where $\alpha(f)$ denotes the transfer function of wave amplitude and the stroke of wave paddle. In the present study, a piston type wave generator is investigated, hence,

$$\alpha(f) = \frac{\sinh kh \cosh kh + kh}{2\sin^2 kh} \tag{10}$$

where, k is the wave number and h is the water depth. Neglecting the excessively small or large period, the associate period resolution can be express as:

$$T_{\min} < T < T_{\max}. \tag{11}$$

Here, $T_{\min} = 0.5$ sec and $T_{\max} = 4.5$ sec are chosen. The surface fluctuations can be expressed as:

$$\zeta(t) = \sum_{n=1}^{N} \sqrt{2 df S(f_n)} \cdot \cos(\sigma_n t - \varepsilon_n), \tag{12}$$

$$\sigma_n = 2\pi f_n, \tag{13}$$

where ε_n and N denotes a random variable number between $0 \sim 2\pi$ and the total number of sampling, respectively.

The horizontal velocities as well as the boundary conditions on the wave-paddle, i.e. Eq. (5), are therefore obtained with

$$U(t) = \sum_{n=1}^{N} \sqrt{2 df S_0(f_n)} \cdot \alpha(f) \cdot \cos(\sigma_n t - \varepsilon_n). \tag{14}$$

2.4 Deployment of Sponge Zone

It is well known that numerical models should have a limited domain. Many researchers resort to

the fact that wave reflection can be reduced by use of some absorption techniques. In this paper we have adopted the idea of an absorbing beach, as shown in Fig. 1. The absorbing beach is composed of two sections: an area with a smoothly varied absorption coefficient μ and an area of constant μ.

Absorption of free surface waves including various conditions is discussed by Cao *et al*. (1993) and Clément (1999); an external pressure in Eq. (4) is specified on the dynamic free surface, and the value of P employed by Grilli (1995) was defined proportional to the normal derivative of the potential energy on the water surface. In the present research, however, as in most approaches suggested earlier, the value of P is defined proportional to the potential on the free water, thus, $P(x, \zeta)$ is expressed as:

$$P(x,\zeta) = \mu(x)\Phi(\xi,\eta,t) \tag{15}$$

where $\mu(x)$ is the beach absorption function, which is assumed to vary smoothly along section $x_x - x_B$, but remain constant after x_x. The absorbing coefficient can be expressed as:

$$\mu(x,t) = \mu_0(t)\rho\left(\frac{x_B - x}{B}\right)^{\alpha}, \qquad x_x < x < x_B \tag{16}$$

$$\mu(x,t) = \mu_0(t)\rho, \qquad x \leqslant x_x \tag{17}$$

where $B = x_x - x_B$ is the length of the varying-value section. As can be seen from Fig. 1, a linear absorption parameter is adopted in this paper, i.e. $\alpha = 1$. It is believed that, by doing so, the results are not seriously affected. The physical meaning of the absorbing area (referred to as the sponge zone) can be representative of various kinds of armor units placed behind the wave flume in reality whose damping coefficient is generally assumed to remain constant and proportioned to the potential energy. The optimized deployment of the sponge zone for periodical, as well as solitary waves was investigated by Chou *et al*. (2002).

2.5 Integral Formulation and Boundary Discretization

According to Green's second identity, the velocity potential $\Phi(x, z; t)$ for inviscid irrotational flow can be obtained by use of the velocity potential on the boundary, $\Phi(\xi, \eta; t)$, and its normal derivative, $\partial\Phi(\xi,\eta;t)/\partial n$. The continuity equation in the differential form, Eq. (1), can thus be transformed into a boundary integral equation:

$$c\Phi(x,z;t) = \frac{1}{2\pi}\int_{\Gamma}\left\{\frac{\partial\Phi(\xi,\eta;t)}{\partial n}\ln\left(\frac{1}{r}\right) - \Phi(\xi,\eta;t)\frac{\partial}{\partial n}\left[\ln\left(\frac{1}{r}\right)\right]\right\}ds \tag{18}$$

$$c = \begin{cases} 1 & \text{inside the fluid domain} \\ 1/2 & \text{on the smooth boundary} \\ 0 & \text{outside the fluid domain} \end{cases}$$

where $r = \sqrt{(\xi - x)^2 + (\eta - z)^2}$.

The boundaries, Γ_1 through Γ_4, are divided into N_1 to N_4 discrete linear elements respectively. When the inner point $(x, z; t)$ approaches the boundary point $(\zeta', \eta'; t)$, the above equation can be written in a discretized form as:

$$\Phi_i(\xi',\eta';t) + \frac{1}{\pi}\sum_{j=1}^{N}\int_{\Gamma_j}\left[\Phi_j(\xi,\eta;t)M_1 + \Phi_{j+1}(\xi,\eta;t)M_2\right]\frac{\partial}{\partial n}\ln\frac{1}{r}ds$$

$$= \frac{1}{\pi}\sum_{j=1}^{N}\int_{\Gamma_j}\left[\frac{\partial\Phi_j(\xi,\eta;t)}{\partial n}M_1 + \frac{\partial\Phi_{j+1}(\xi,\eta;t)}{\partial n}M_2\right]\ln\frac{1}{r}\mathrm{d}s \tag{19}$$

where, $r=\sqrt{(\xi-\xi')^2+(\eta-\eta')^2}$; $M_1=(1-\chi)/2$; $M_2=(1+\chi)/2$, M_1 and M_2 being the shape function within χ, the local dimensional coordinate. Hence, for the operation of calculation, Eq. (19) can be expressed in the matrix form:

$$[\Phi_i] = [O_{ij}][\bar{\Phi}_i]; \quad i,j = 1 \sim 4 \tag{20}$$

where $[\Phi]$ and $[\bar{\Phi}]$ are, respectively, the velocity potential and its associated normal derivative. The coefficients of the matrix $[O]$ are related to the geometric shapes of the boundaries. Detailed expressions of the numerical scheme and these matrixes are given in Chou and Shih (1996a, 1996b).

Two discretization schemes are used in the analysis to test the effects of the sizes of the meshes. A rather fine temporal resolution is chosen primarily with $\Delta t = 0.0025$ s, and a resolution of $\Delta t = 0.005$ s is adopted subsequently. On the other hand, for the saving of computer storage and computation time, the spatial resolutions are varied. Coarser meshes are used at both ends of the flume, and they are then varied gradually when approaching the middle of the flume. The smallest mesh sizes adopted for the computation are, respectively, $\Delta x = 0.05h$ for the former case, and $\Delta x = 0.10h$ for the latter, h being the water depth. The discretization schemes are exhaustive in Figs. 2(a) and 2(b).

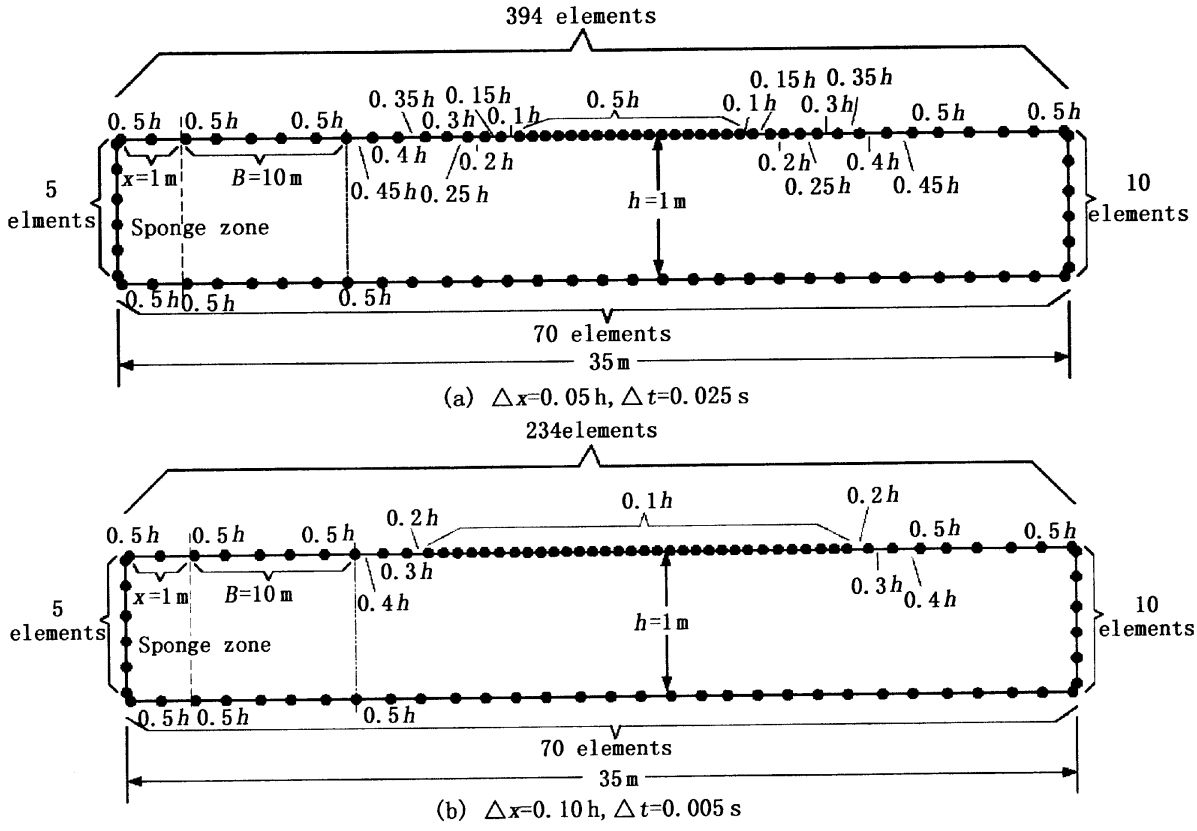

Fig. 2. Discretization scheme.

The time histories of surface elevations are measured by a total of 14 pseudo wave gauges, and the

measuring stations are used to record the developments of irregular waves along the wave tank. Hereafter they will be called, starting from the wave-paddle, Station 1 ~ Station 14. Table 1 lists the number of the stations and their distances from the origin.

Spectral analyses are carried out in the usual way as were done for field data. The wave records are first checked for possible outliers (Chen and Ma, 1991), which may result from the sudden breakdowns of the computer during simulations. Once a possible outlier is detected it will be corrected according to a procedure proposed by Chen and Ma (1991). Afterwards, the wave records are divided into segments with 50% over-lapping. In this way the degrees of freedom (DOF) in the spectral estimates can be largely increased (Otnes and Enochson, 1972). A partial cosine taper function is also added to each segment so that side-lobe leakage can be minimized (Bendat and Piersol, 1986). However, it is believed that since the "wave records" is relatively short, and contain fewer waves than field data, these procedures could, at least, increase the degrees of freedom of the spectral estimates.

Table 1 The pseudo wave stations and their locations

Station No.	Case A	Case B
	Distance from the origin (m)	Distance from the origin (m)
1	29.95	31.3
2	28.95	30.3
3	27.95	28.3
4	26.95	26.3
5	25.95	25.3
6	24.95	24.3
7	22.95	22.3
8	21.95	20.3
9	20.95	18.3
10	19.95	17.3
11	17.95	16.3
12	15.95	15.3
13	13.95	14.3
14	11.95	12.3

Each segment was separately Fast Fourier Transformed (FFT), and a rough, two-sided spectral estimate can be obtained. Smooth estimate of the spectral densities is obtained through ensemble averaging. The Hanning window applied in the frequency domain leads to the final smoothing of the spectral densities (Bendat and Piersol, 1986). Depending upon the discretization time intervals of the wave records, Δt, the DOF of the spectral estimates ranges from 2 to 68, with the corresponding frequency resolution in the range of $\Delta f = 0.00976563 \sim 0.3125$ Hz.

3. Results and Discussion

3.1 Efficiency of Absorption

Fig. 3 shows a comparison of the time histories of random wave generation with and without absorption technique, i.e. $\mu = 1.0$ and $\mu = 0.0$, respectively. The efficiency of absorption for regular and solitary waves has been investigated by Chou *et al.* (2002); a value of $\mu = 1.0$ gives satisfactory results for both solitary and regular waves. However, the same coefficient might not be well employed for train of irregular waves; therefore, even though an absorbing technique is employed in the model, still, a small number of waves reflected from the vertical wall and the wave paddle inevitably contaminate the incident wave train. As can be seen from Fig. 3(a), partial reflection of irregular short-crested and/or long-crested finite-amplitude waves is formed in the vicinity of the vertical wall, whereas this appearance is not conspicuous in Fig. 3(b). Fig. 4 reveals the efficiency of absorption for irregular waves in a 3-dimensional graphic corresponding to Fig. 3.

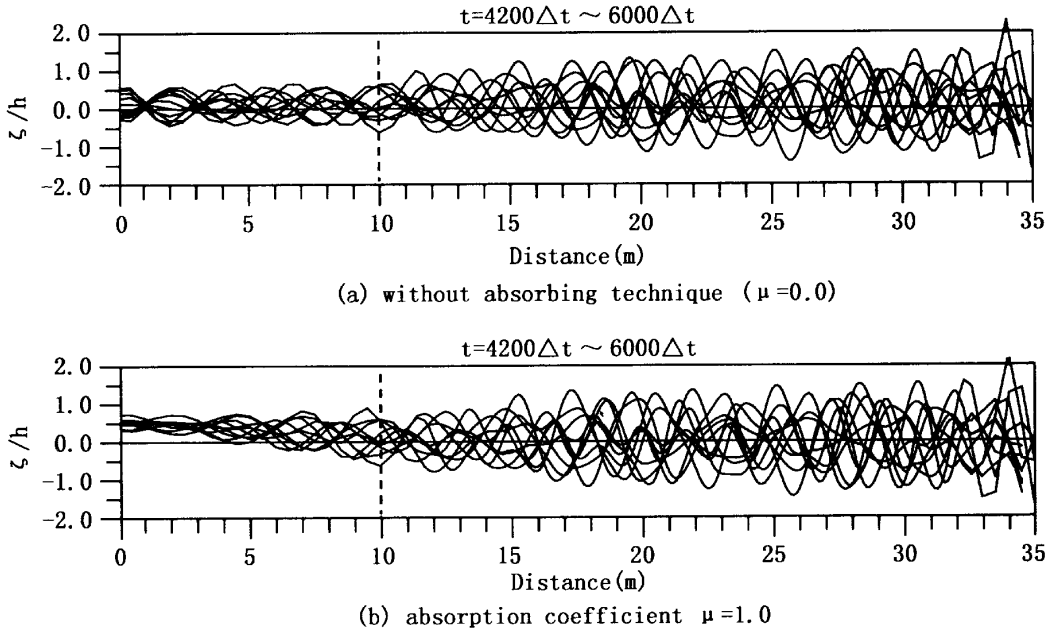

Fig. 3. Comparison between the time histories of the developments of irregular waves along the numerical wave tank.

3.2 Effects of Peak Frequency

Fig. 5 reveals the surface fluctuations of random waves measured by the fourteen pseudo gauges, and the corresponding spectra are shown in Fig. 6. The significant wave height $H_{1/3}$ and the significant wave period $T_{1/3}$ are 2.5 cm and 0.8 sec, respectively. This is the case with the highest peak frequency considered in all the numerical simulations. The temporal discretization step used is Δt = 0.0025 sec, with the smallest mesh size of $\Delta x = 0.05h$.

It can be seen from Fig. 5, starting from Station No.7, at approximately 20 seconds, a wave group with a permanent form seems to have been formed. This wave group keeps its identity and travels

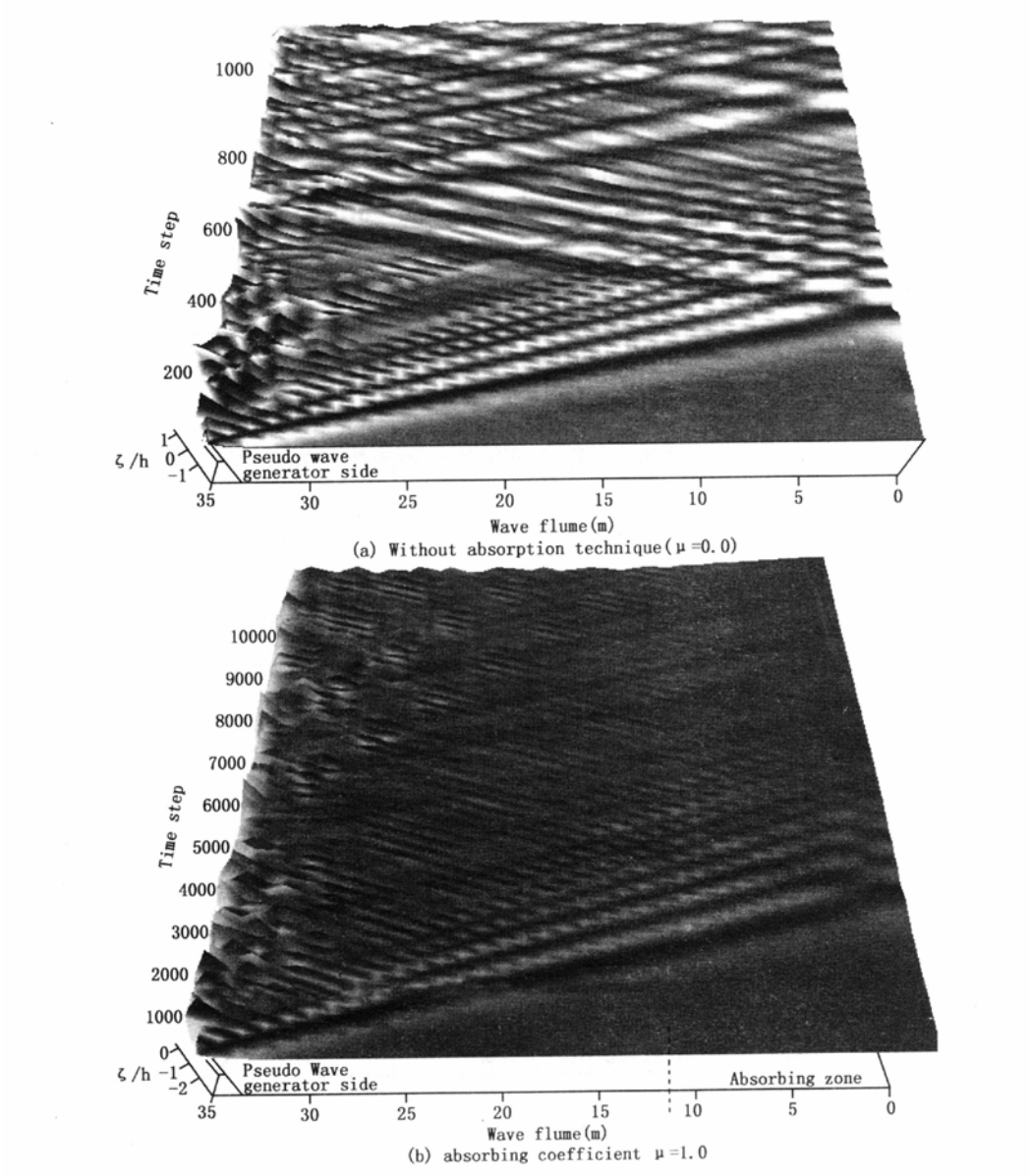

Fig. 4. 3-Dimensional sketch of the developments of irregular wave propagation along the wave flume.

down to the end of the flume. This occurrence is interesting, since it is well known that, for deep water waves, the effects of nonlinear wave-wave interactions, and thus the transfer of energy between wave components, occur at the third order of the wave steepness (Phillips, 1981). Wave groups with permanent forms, or solitons, are known to form in wave trains having a "carrier frequency" (Yuen and Lake, 1982). As shown by Hasselmann (1962), for irregular waves with a Neumann-type spectrum, which is equivalent in form to the Mitsuyasu-Bretschneider spectrum used here, energy transfer occurs only at the fifth order. It is therefore concluded that the wave group seen in Fig. 5 is not the result of nonlinear wave-wave interaction. However, further investigations are needed to clarify this phenomenon. From Fig. 6, it is seen that wave energy decreases as waves propagate toward the end of the flume. This, however, is not the result of the absorbing beach, as can be seen from the figures to be

presented later.

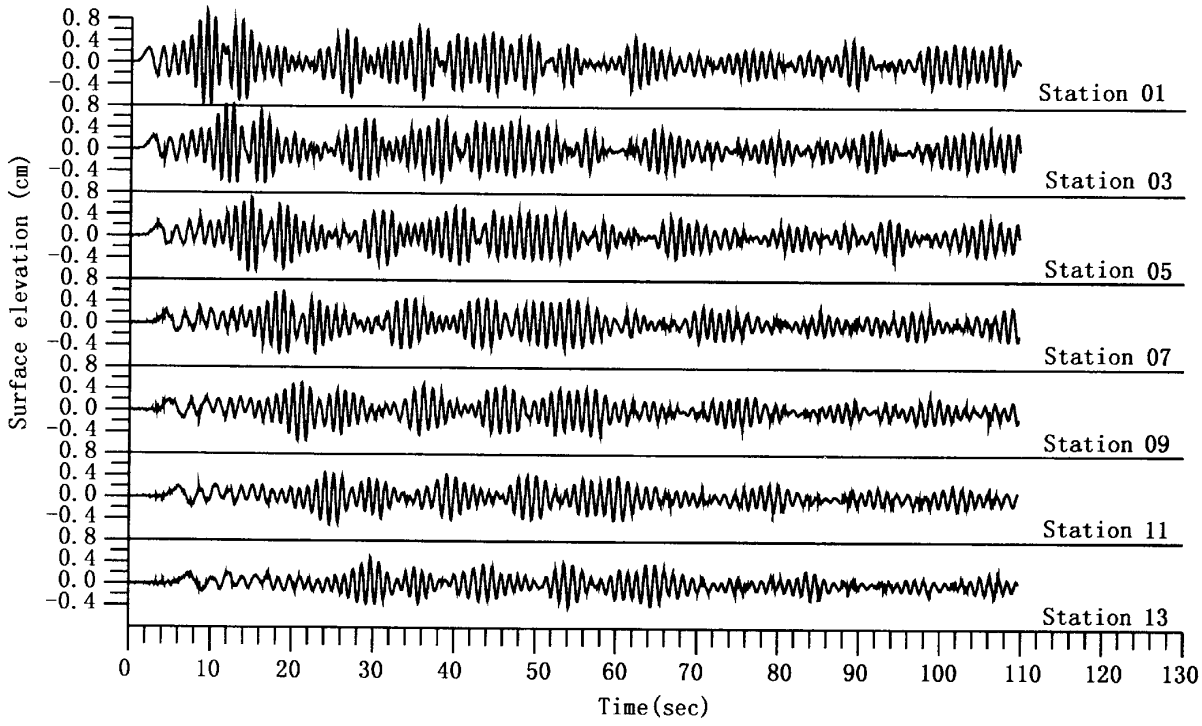

Fig. 5. Developments of irregular waves advancing from Station Nos. 1 ~ 13.
The conditions are: significant wave height $H_{1/3}$ = 2.5 cm, significant wave period $T_{1/3}$ = 0.8 sec, Δt = 0.0025 sec, and Δx_{min} = 0.05h.

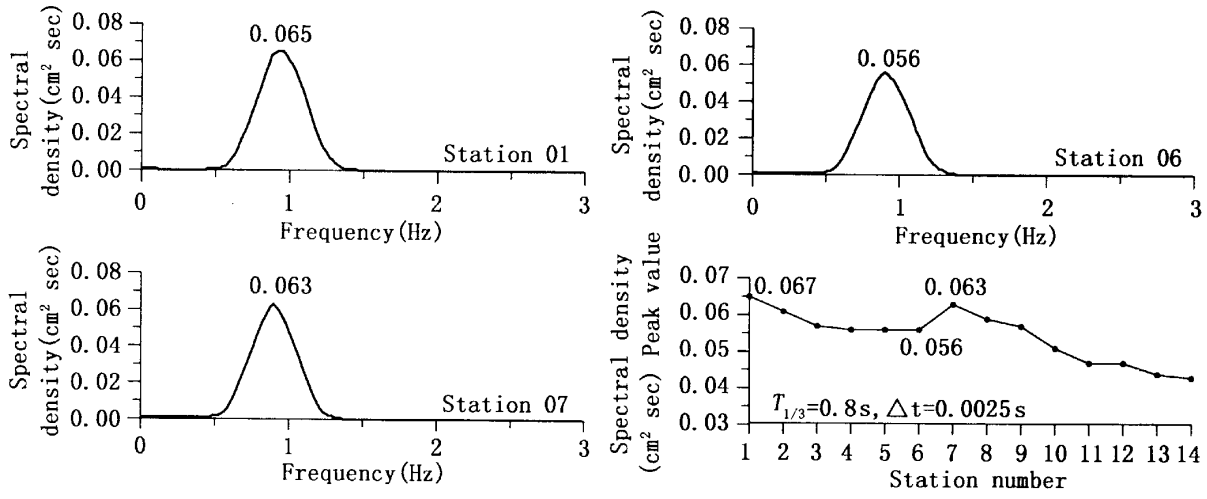

Fig. 6. Spectra of irregular waves and the variation along the numerical wave tank.
The conditions are: significant wave height $H_{1/3}$ = 2.5 cm, significant wave period $T_{1/3}$ = 0.8 sec, Δt = 0.0025 sec, and Δx_{min} = 0.05h.

Figs. 7 and 8 show the developments of those waves with a significant wave period of $T_{1/3}$ = 1.1 sec. The discretization scheme used for this case is the same as that of Fig. 5. Since the Mitsuyasu-Bretschneider spectrum is an empirical formula based on wave records measured on the open sea, the energy level of this spectrum increases with the decreasing value of the peak frequency. As a result,

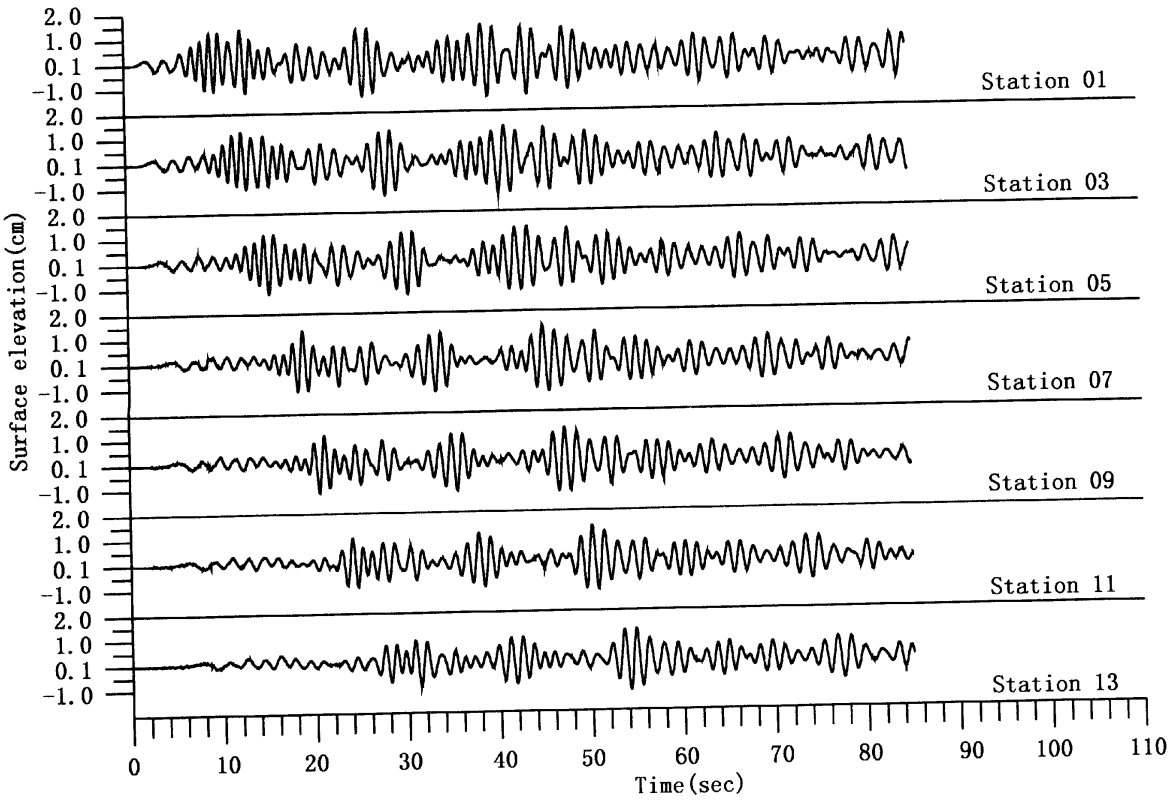

Fig. 7. Developments of irregular waves advancing from Station Nos. 1 ~ 13. The conditions are: significant wave height $H_{1/3}$ = 2.5 cm, significant wave period $T_{1/3}$ = 1.1 sec, Δt = 0.0025 sec, and $\Delta x_{min} = 0.05h$.

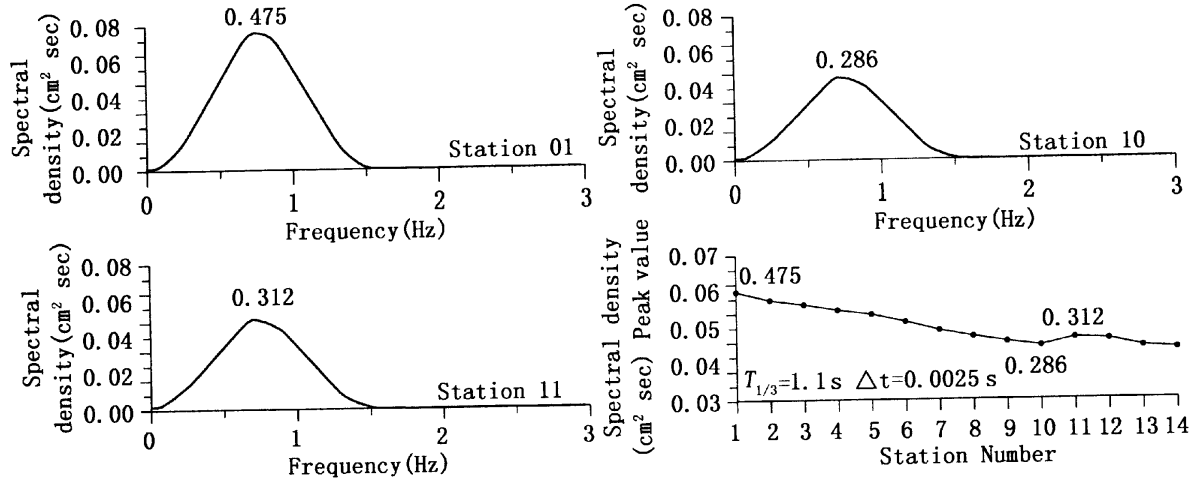

Fig. 8. Spectra of irregular waves and the variation along the numerical wave tank. The conditions are: significant wave height $H_{1/3}$ = 2.5 cm, significant wave period $T_{1/3}$ = 1.1 sec, Δt = 0.0025 sec, and $\Delta x_{min} = 0.05h$.

waves in Fig. 7 have larger wave heights than those in Fig. 5. Notice also that, although the energies

of the waves diminish as they propagate down the flume, some of those last four stations, as shown in Fig. 8 and are found to have higher spectial densities than those at Station Nos. 8 ~ 10. This fact can also be seen later in Fig. 12, where the spectral variations for all the fourteen stations are also shown. It is conjectured that this is due to the presence of partially reflected long waves from the numerical beach. As these wave groups begin to depart from each other, high frequency waves are thus "generated" between these wave groups. Whether these high-frequency waves correspond to the "false waves", as called by Giménez *et al.* (1994; see also Pires-Silva and Medina, 1994), is presently uncertain. It should be noted that, to avoid numerical instability, the discretization time steps should be small, and any small fluctuation could be treated as a high-frequency wave. Since the frequency resolution is closely related to the discretization time step, a small Δt will inevitably lead to a small Δf; thus, a combination of these two effects could and is expected to add inaccuracies to the present numerical results. Through comparison of Figs. 6 and 8, it is concluded that, in the present numerical scheme, the energy of high frequency waves decreases more rapidly than that of low frequency waves.

3.3 Effect of the Discretization Scheme

The quantity of discrete elements determines the simulating time. By use of a 2.8 GHz CPU personal computer, it takes about 15 sec per time-step for mesh sizes of $\Delta x = 0.05h$; yet it only takes approximately 4 sec per time-step for $\Delta x = 0.10h$. Figs. 9 ~ 12 demonstrate the effect of a coarse

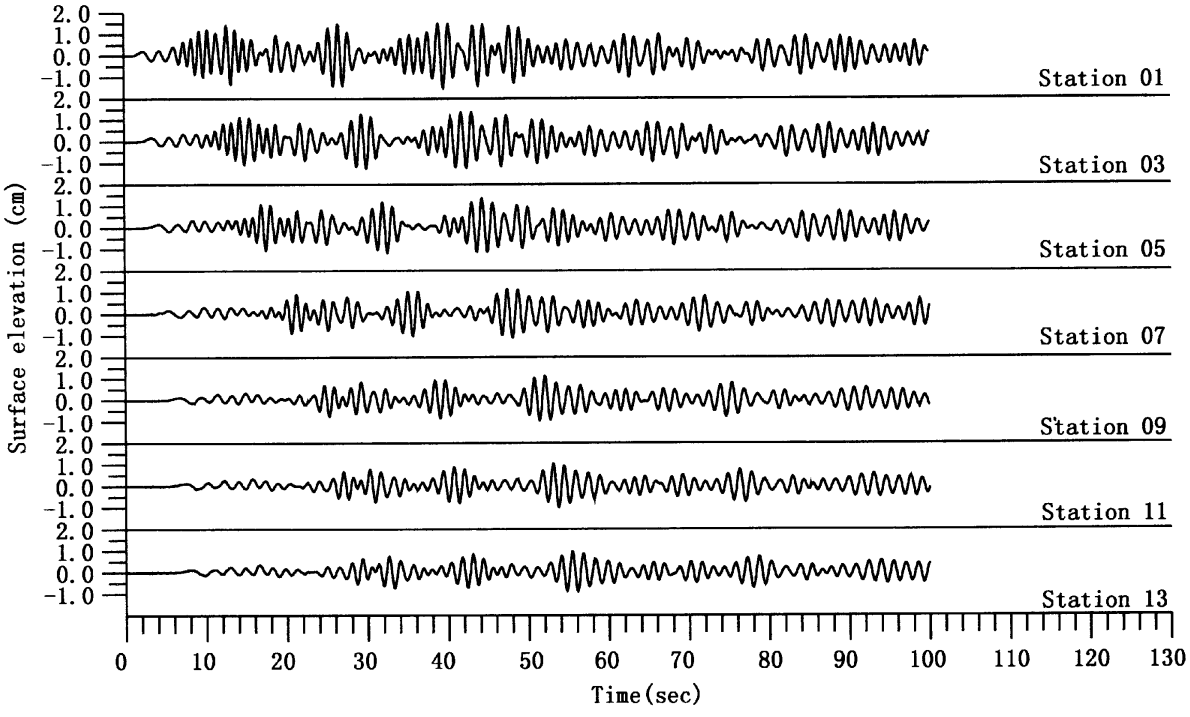

Fig. 9. Developments of irregular waves advancing from Station Nos. 1 ~ 13. The conditions are: significant wave height $H_{1/3} = 2.5$ cm, significant wave period $T_{1/3} = 1.1$ sec, $\Delta t = 0.005$ sec, and $\Delta x_{min} = 0.10h$.

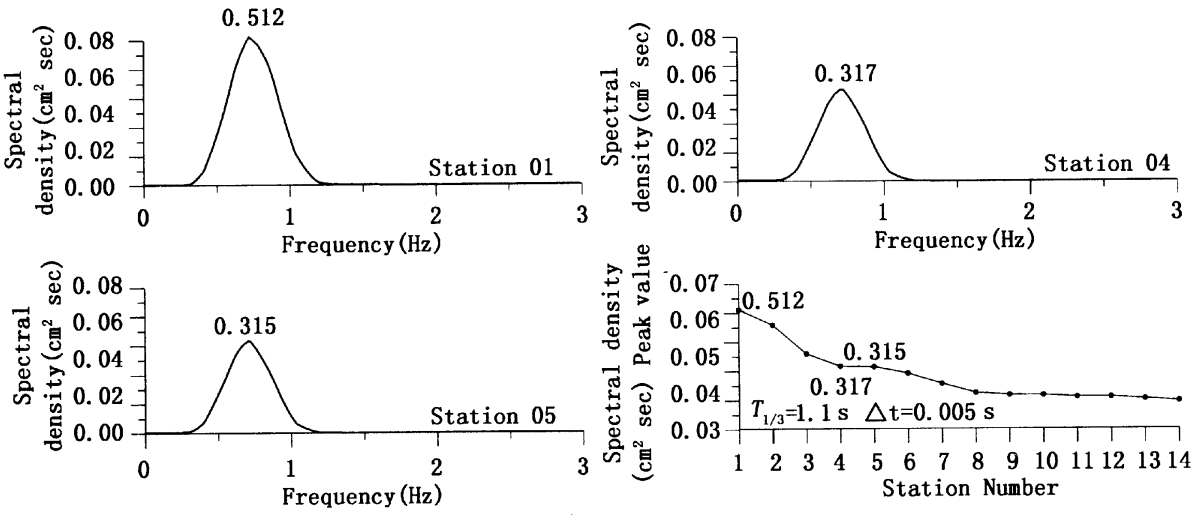

Fig. 10. Spectra of irregular waves and the variation along the numerical wave tank. The conditions are: significant wave height $H_{1/3}$ = 2.5 cm, significant wave period $T_{1/3}$ = 1.1 sec, Δt = 0.005 sec, and $\Delta x_{min} = 0.10h$.

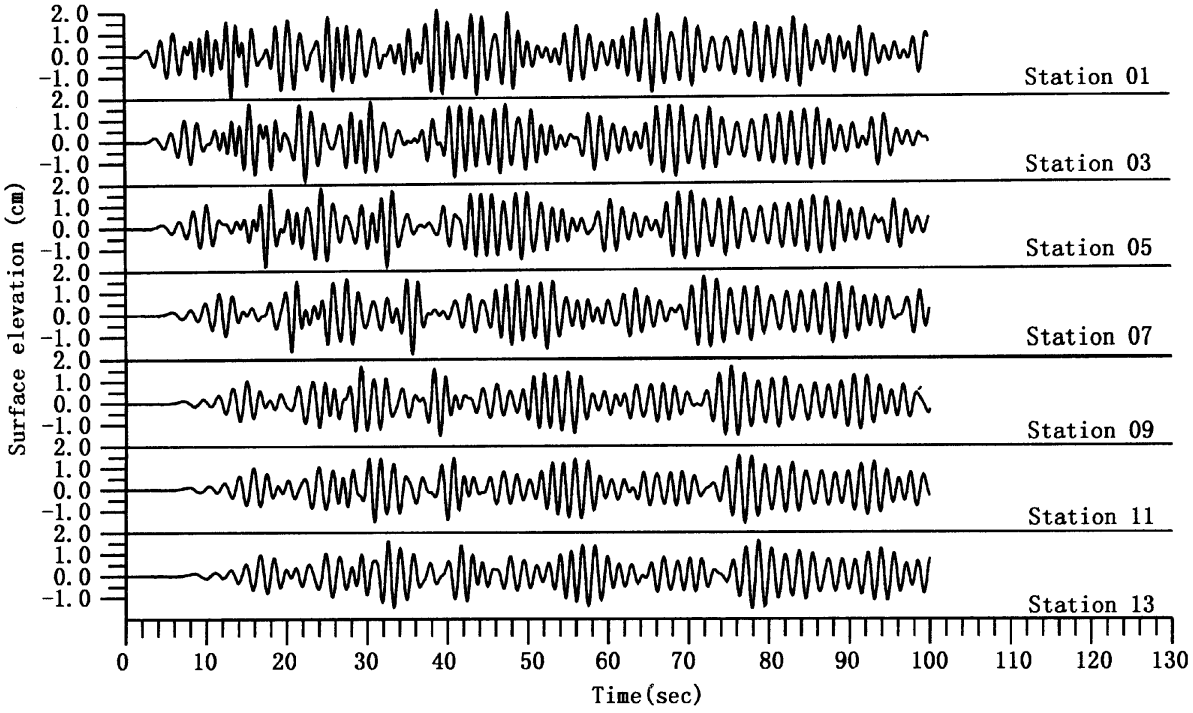

Fig. 11. Developments of irregular waves advancing from Station Nos. 1 ~ 13. The conditions are: significant wave height, $H_{1/3}$ = 2.5 cm, significant wave period $T_{1/3}$ = 1.4 sec, Δt = 0.005 sec, and $\Delta x_{min} = 0.10h$.

discretization scheme. Figs. 9 and 10 are for a short significant wave period of $T_{1/3}$ = 1.1 sec, whereas Figs. 11 and 12 are for $T_{1/3}$ = 1.4 s. Even though the same significant wave period is used, it seems that more waves are generated in Fig. 9 than in Fig. 7. A comparison of Figs. 10 and 12 leads to a similar conclusion, that is, waves with higher peak frequencies decrease faster in energy

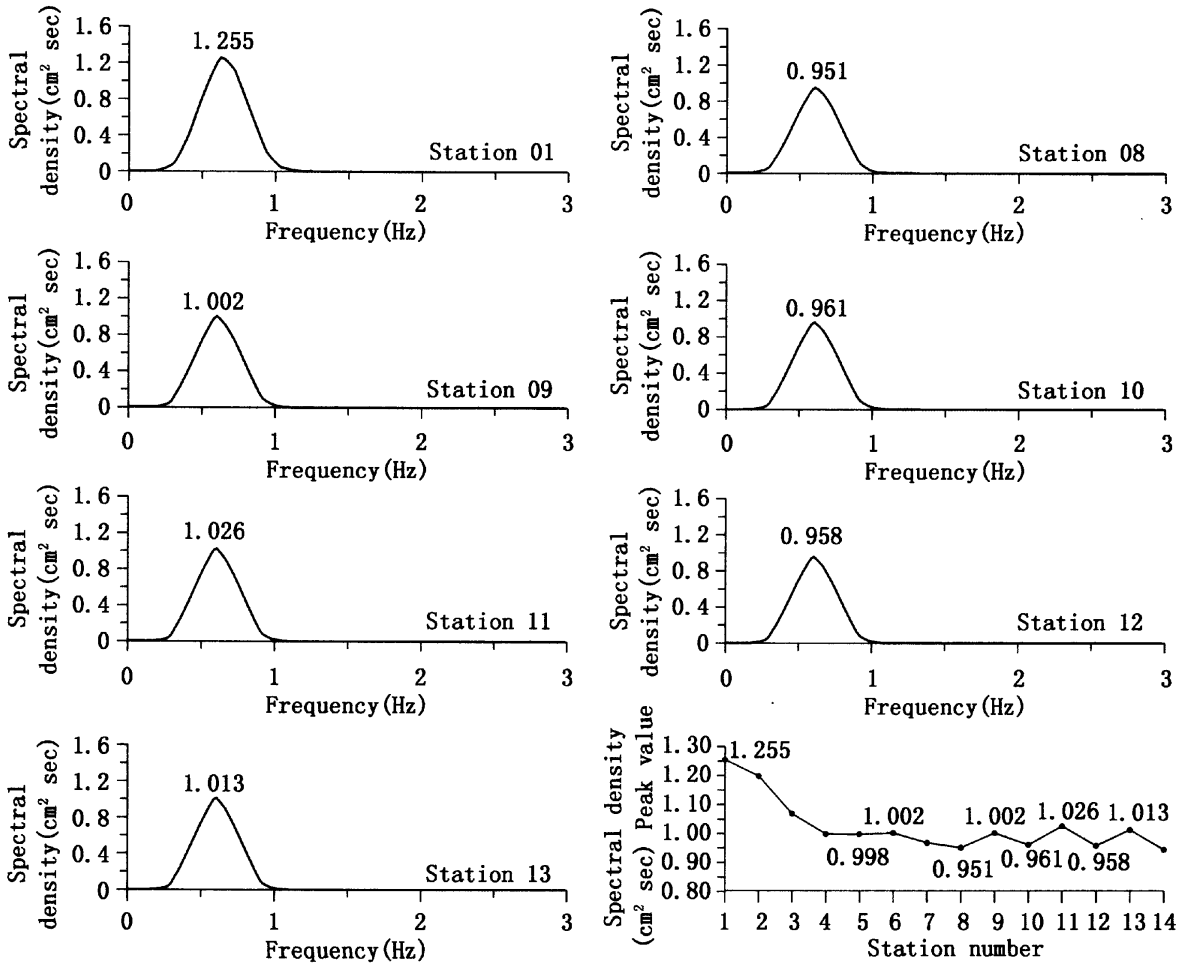

Fig. 12. Spectra of irregular waves and the variation along the numerical wave tank. The conditions are: ficant wave height $H_{1/3}$ = 2.5 cm, significant wave period $T_{1/3}$ = 1.4 sec, Δt = 0.005 sec, and $\Delta x_{\min} = 0.10h$.

than low frequency waves.

The total length of our wave flume is 35 meters, as mentioned previously, and the first 20 meters are for the propagation of irregular waves. For a wave spectrum with a significant wave period of $T_{1/3}$ = 1.1 seconds, the corresponding characteristic wavelength is $\lambda_p \approx 1.96$ m. Depending on the significant wave periods, our computation time is in the range of 80 to 120 seconds. According to Xu and Baddour's (1999) review, the space domain of their computation is typically 10 times the characteristic wavelength for simulating the generation and propagation of nonlinear, irregular waves, and their typical simulation runs for at least 200 characteristic wave periods. Correspondingly, both the time and space domains of our computation conform to those of Xu and Baddour; as a result, our numerical scheme is comparable. However, unlike the results of Xu and Baddour, who applied the Green-Naghdi fluid sheets theory, the present results are obtained by solving the nonlinear governing equations directly, and thus are believed to be more general.

4. Conclusions

The generation and propagation of nonlinear random waves in a wave tank are studied numerically with the boundary element method. A Bretschneider-Mitsuyasu type spectrum is used as the target spectrum for irregular waves. The waves are generated by a piston-type wave generator installed at one end of the flume, and are dissipated by a numerical absorbing beach at the other end of the flume.

Some conclusions may be drawn from the present study:

(1) Even though a relatively small discretization scheme, both spatially and temporally, are used, as the waves propagate toward the end of the flume, the wave energies are seen to be diminished. This is true, no matter whether the waves have a large or a small significant wave period. For waves with a large significant wave period, i.e., a low peak frequency, the energy decreases faster than for waves with a small significant wave period.

(2) Since only one absorbing beach is used at the left end of the flume, low frequency waves seem to have been reflected from the beach. This could explain at least in part, the reason why energies at the last four stations increase, instead of decreasing.

(3) During simulations, waves of very high frequencies can be generated. This is probably due to the fact that extremely small discretization steps are used in the analyses. The smallness of the discretization steps can have the effect of generation of the so-called false waves on the one hand, and increase the frequency resolution on the other. This is believed to be necessary, however, to maintain the numerical stability of the present scheme.

(4) In some cases, wave groups with permanent forms appear to have been formed during propagation. However, since the time for wave-wave interaction, and therefore for energy transfer between wave components, is too short, it can be concluded that the appearance of wave groups with permanent forms is only an artifact.

(5) In general, all the spectra from the fourteen measuring stations have an appearance similar to that of the target spectrum. This is due to the fact that there are more simulated waves in the flume than in the results of other researchers. It is believed that, albeit further improvements are necessary, our algorithm is capable of simulating the generation and propagation of nonlinear random waves.

References

Bendat, J. S. and Piersol, A. G., 1986. *Random data Analysis and Measurement procedures*, 2nd ed., John Wiley, New York, N.Y., pp. 566.

Brorsen, M. and Larsen, J., 1987. Source generation of nonlinear gravity waves with the boundary integral equation method, *Coastal Engineering*, **11**(4): 93 ~ 113.

Cao, Y., Beck, R. F. and Schultz, W. W., 1993. An absorbing beach for numerical simulations of nonlinear waves in a wave tank, *Proc. 8th Int. Workshop Water Waves and Floating Bodies*, 17 ~ 20.

Chen, S.-J. and Ma, G.-R., 1991. *Methods of oceanographic data analyses and their applications*, Ocean Publication Co., Beijing, pp. 660. (in Chinese)

Chou, C. R. and Shih, R. S., 1996a. Generation and deformation of solitary waves, *China Ocean Engineering*, **10**(4): 419 ~ 432.

Chou, C. R. and Shih, R. S., 1996b. Numerical generation and propagation of periodical waves in time domain, *Coastal Engineering in Japan*, **39**(2): 111 ~ 127.

Chou, C. R., Shih, R. S. and Yim, J. Z., 2001. A numerical wave tank for nonlinear waves with passive absorption, *China Ocean Engineering*, **15**(2): 253 ~ 268.

Chou, C. R., Shih, R. S. and Yim, J. Z., 2002. Optimizing deployment of sponge zone on numerical wave channel, *Journal of the Chinese Institute of Engineering*, **25**(2): 147 ~ 156.

Clément, A. H., 1999. Benchmark test cases for numerical wave absorption: 1st Workshop of ISOPE numerical wave tank group, Montréal, May 1998, *Proc. 9th Int. Offshore and Polar Eng. Conf.*, Brest, Vol. Ⅲ, 266 ~ 289.

Giménez, M. H., Sánchez-Carratalá, C. R. and Medina, J. R., 1994. Analysis of false waves in numerical sea simulations, *Ocean Engng.*, **21**, 751 ~ 764.

Goda, Y., 2000. *Random seas and design of maritime structures*, 2nd ed., World Scientific, Singapore, 443.

Grilli, S. T. and Horrillo, J., 1997. Numerical generation and absorption of fully nonlinear periodic waves, *J. Eng. Mech.*, ASCE, **123**, 1060 ~ 1069.

Gudmestad, O. T. and Spidsøe, N., 1990. Deep water wave kinematic models for deterministic and stochastic analysis of drag dominated structures, in: A. Tørum and O. T. Gudmestad (eds.) "*Water wave kinematics*" Proc. NATO Advanced Research Workshop on Water Wave Kinematics Model, Norway, Kluwer Academic Publishers, Dordrecht, pp. 57 ~ 87.

Hasselmann, K., 1962. On the non-linear energy transfer in a gravity-wave spectrum(Part 1: General theory, *J. Fluid Mech.*, **12**, 481 ~ 500.

Isaacson, M., Cheung, K. F., Mansard, E. and Miles, M. D., 1993. Transient wave propagation in a laboratory flume, *J. Hydraulic Res.*, **31**, 665 ~ 680.

Johnson, R. S., 1972. Some numerical solutions of a variable-coefficient Korteweg-de Vries equation (with applications to solitary wave development of a shelf), *J. Fluid Mech.*, **54**, 81 ~ 91.

Otnes, R. K. and Enochson, L., 1972. *Digital time series analysis*, John Wiley and Sons, New York, pp. 467.

Pires-Silva, A. A. and Medina, J. R., 1994. False waves in wave records, *Ocean Engng.*, **21**, 765 ~ 770.

Phillips, O. M., 1981. Wave interactions(the evolution of an idea, *J. Fluid Mech.*, **106**, 215 ~ 227.

Sugino, R. and Tosaka, N., 1990. Boundary element analysis of nonlinear water wave problem, *Proc. of the Pacific Congress on Marine Science and Technology*, PACON, **90**, 18 ~ 25.

Tørum, A. and Skjelbreia, J. E., 1990. *Irregular water wave kinematics*, in: A. Tørum and O. T. Gudmestad (eds.), "*Water wave kinematics*", Proc. NATO Advanced Research Workshop on Water Wave Kinematics Model, Norway, Kluwer Academic Publishers, Dordrecht, pp. 281 ~ 295.

Williams, A. N., 1999. *Simulation of the generation and propagation of second-order Stokes waves in a two-dimensional wavetank*, in: Nonlinear water wave interaction, O. Mahrenholtz and M. Markiewicz (eds.), WIT Press, Southhampton, UK, pp. 167 ~ 197.

Xu, Q. and Baddour, R. E., 1999. Modeling nonlinear irregular waves in a numerical basin, *Int. Workshop on Natural Disaster by Storm Waves and Their Reproduction in Experimental Basin*, (*Wave Generation* '99), Nov. 30 ~ Dec. 3, 1999, Kyoto, Japan, pp. 151 ~ 159.

Yuen, H. C. and Lake, B. M., 1982. Nonlinear dynamics of deep-water gravity waves, *Adv. Appl. Mech.*, **22**, 67 ~ 229.